Topological Approach of Characterizing Optical Skyrmions and Multi-Skyrmions

Amy McWilliam, Claire M. Cisowski, Zhujun Ye, Fiona C. Speirits, Jörg B. Götte, Stephen M. Barnett, and Sonja Franke-Arnold*

The skyrmion number of paraxial optical skyrmions can be defined solely via their polarization singularities and associated winding numbers, using a mathematical derivation that exploits Stokes's theorem. It is demonstrated that this definition provides a robust way to extract the skyrmion number from experimental data, as illustrated for a variety of optical (Néel-type) skyrmions and bimerons and multi-skyrmions. This method generates not only an increase in accuracy, but also provides an intuitive geometrical approach to understanding the topology of such quasi-particles of light and their robustness against smooth transformations.

1. Introduction

The concept of skyrmions was proposed by Skyrme over 60 years ago,[1] originally postulated to describe the topological structure of nucleons. Since then, these quasi-particles have been predicted and observed in a wide range of contexts, including string theory,[2] Bose-condensates and atoms,[3,4] spintronics,[5] magnetic media,[6–8] and more recently in plasmonics and optics.[9–13] While the more familiar magnetic skyrmions carry magnetic spin textures, optical skyrmions are embedded in the polarization texture of complex vector light fields. Of particular interest to the experimentalist are 2D skyrmions, sometimes called 'baby skyrmions', which can be realized in paraxial beams, offering an easily accessible and re-configurable platform for the investigation of topological features and their propagation dynamics.[14–19] Unlike magnetic skyrmions, freely propagating paraxial optical skyrmions are only constrained by Maxwell's equations, and therefore offer a versatile platform for the investigation of exotic topological structures.[20] The generation of topological states of light opens up new avenues for the controlled interaction of photons with material quasi-particles such as plasmons, phonons, and excitons.[21]

Experimentally, polarization textures and hence skyrmions can be assessed by measuring the spatially varying reduced Stokes vector $\mathbf{S}(x, y)$ across the light profile, mapping the local polarization states onto the Poincaré sphere, just like the local spin of magnetic skyrmions is mapped onto the Bloch sphere.[22] The polarization texture itself can take on almost unlimited shapes, including Néel-type (hedgehog) and Bloch-type skyrmions,[12,15,20,23,24] but the underlying topology is characterized by a single invariant, the skyrmion number, n, which counts how many times $\mathbf{S}$ wraps around the Poincaré sphere.[Note that while every Skyrmion beam is a Poincaré beam, the reverse does not hold: The mapping must obey specific mapping rules. This is intrinsic to the definition of the Skyrmion number, Equation (1) but becomes more evident from our geometric description in this letter]. While the polarization structure of a beam may change upon propagation in free space and through unitary transformations, n remains conserved.

Both isolated optical skyrmions and and more complex geometries with multiple optical skyrmions can be generated with state-of-the-art light-shaping technology. Their experimental identification in terms of their skyrmion number, however, remains challenging. Previous work has relied either on a qualitative comparison between measured and ideal polarization profiles of the target skyrmion, or evaluated the skyrmion number from its analytical expression, which for a beam propagating along the z direction, is defined as[25]

$$n = \frac{1}{4\pi}\int_A \mathbf{S}\cdot\left(\frac{\partial \mathbf{S}}{\partial x}\times\frac{\partial \mathbf{S}}{\partial y}\right)dxdy \tag{1}$$

where $\mathbf{S} = [S_1, S_2, S_3]^T$ is the spatially resolved normalized reduced Stokes vector, and A is the entire (x, y) plane. The skyrmion number is thus, by definition, a global property of a light beam. Evaluating Equation (1) poses two difficulties: first, the experimentally accessible part of A is limited by the numerical aperture of the system. Second, gradients are notoriously sensitive to noise, especially in low intensity regions, such as at large radial distances or in the vicinity of singularities, where the spatial derivative of fluctuating noise levels may overwhelm the signal.

In this research article, we derive and demonstrate an alternative, topological method to calculate skyrmion numbers

A. McWilliam, C. M. Cisowski, Z. Ye, F. C. Speirits, J. B. Götte, S. M. Barnett, S. Franke-Arnold
School of Physics and Astronomy
University of Glasgow
GlasgowG12 8QQ, UK
E-mail: a.mcwilliam.1@research.gla.ac.uk

The ORCID identification number(s) for the author(s) of this article can be found under https://doi.org/10.1002/lpor.202300155

DOI: 10.1002/lpor.202300155

that avoids products of polarization gradients and significantly increases precision (for low n) and accuracy (in the presence of noise). We evaluate n for a variety of experimentally generated optical skyrmions and multi-skyrmions, the latter being constructed by combining multiple skyrmions cores as discussed in[20] and.[26] Our method provides geometric insight that is missing from the surface integral representation: allowing us, for example, to interpret multi-skyrmions as combination of individual skyrmion structures rather than just providing an overall skyrmion number. This method can be extended to analyze skyrmion lattices with periodic structures.

2. Results and Discussion

2.1. Topological Definition of The Skyrmion Number

We start by deriving our topological definition from the integral definition of Equation (1). For paraxial beams, the skyrmion number can be interpreted as the integrated flux of a skyrmion field $\mathbf{\Sigma}$, sometimes known as the topological current, across the transverse plane,

$$n = \frac{1}{4\pi}\int_A \mathbf{\Sigma}\cdot d\mathbf{A} \tag{2}$$

where $\Sigma_i = \frac{1}{2}\epsilon_{ijk}\epsilon_{pqr}S_p(\partial_j S_q)(\partial_k S_r)$ and ∂_i denotes differentiation with respect to x_i.[12] Here, $\mathbf{S}_R = (S_x, S_y, S_z)^T$ is a generalized Stokes vector that relates to the conventional Stokes vector through an arbitrary rotation, described by a 3D rotation matrix R, so that $\mathbf{S}_R = R\mathbf{S}$.[24]

The skyrmion field $\mathbf{\Sigma}$ is transverse ($\nabla\cdot\mathbf{\Sigma} = 0$), hence it can be expressed as the curl of a vector field $\mathbf{v}$. Applying Stokes's theorem yields

$$n = \frac{1}{4\pi}\int_A \nabla\times\mathbf{v}\cdot d\mathbf{A} = \frac{1}{4\pi}\oint_C \mathbf{v}\cdot d\boldsymbol{l} \tag{3}$$

where C is a suitable integration path across A, which excludes any singularities of $\mathbf{v}$. While $\mathbf{v}$ is not uniquely defined, a suitable expression in terms of the experimentally accessible Stokes parameters is

$$\mathbf{v} = -S_z\nabla\Phi, \quad \text{where} \quad \Phi = \arg(S_x + iS_y) \tag{4}$$

Equation (4) can be derived by recalling the Mermin and Ho relation,[27,28] but for our purposes it is sufficient that its curl is indeed the skyrmion field $\mathbf{\Sigma}$.

The skyrmion number can then be expressed as a line integral

$$n = -\frac{1}{4\pi}\oint_C S_z\nabla\Phi\cdot d\boldsymbol{l} \tag{5}$$

which depends only on the variation of the phase Φ along the path. The integration path has to enclose the entire (in principle infinitely extended) beam area, but exclude all singularities, as illustrated in **Figure 1**. The integrals connecting the beam periphery to the singularities cancel. This leaves us with two (or more) closed line integrals: one at a radius $\rho\to\infty$, evaluated counter-clockwise (α), and one or more around the singularities of Φ, evaluated in a clockwise direction (β_j):

$$n = \sum_j \frac{1}{4\pi}\oint_{\beta_j} S_z\nabla\Phi\cdot d\boldsymbol{l} - \frac{1}{4\pi}\oint_\alpha S_z\nabla\Phi\cdot d\boldsymbol{l} \tag{6}$$

At the positions of the j^{th} inner singularity (x_j, y_j) the Stokes parameter is simply the local value $S_z^{(j)}$, and can be taken out of the integral. At the beam periphery the Stokes parameter converges to a single value $\bar{S}_z^{(\infty)}$, because the skyrmion beam carries a finite energy. Each integral is related to the winding number $N = (2\pi)^{-1}\oint\nabla\Phi\cdot d\boldsymbol{l}$, which counts the number of turns $\mathbf{S}$ completes on the Poincaré sphere along the respective circular paths and by definition is free from noise. We thus obtain a topological definition of the skyrmion number,

$$n = \frac{1}{2}\left(\sum_j S_z^{(j)}N_j - \bar{S}_z^{(\infty)}N_\infty\right) \tag{7}$$

which is a function of the Stokes vector at the position of the singularities and at the beam periphery, and the corresponding integer winding numbers on the Poincaré sphere. It is straightforward to show that $N_\infty = \sum_j N_j$, therefore, guaranteeing that n is an integer. Additional details of the derivation of Equation (7) are provided in Section A of the Supporting Information. As $\mathbf{\Sigma}$ is invariant under rotations, the skyrmion number n does not depend on the orientation of the Poincaré sphere, giving us unlimited options of choosing $\mathbf{S}_R$ when calculating n.

We will now illustrate how Equation (7) links to the topology of the polarization texture using the example of an $n = 2$ skyrmion (of the form $|\Psi_2\rangle$ of Equation (8) introduced later in this article). Figure 1a shows the polarization texture, with local polarization states color-mapped to the Poincaré sphere as indicated in the inset, along with the corresponding vectorial representation of $\mathbf{S}(x, y)$. If we choose $\mathbf{S}_R = (S_1, S_2, S_3)$, as illustrated in Figure 1b, the polarization profile features a left-handed C-point singularity in the center,[29] and a delocalized right-handed singularity at the beam periphery, as identified by the phase profile Φ. A suitable path integral, indicated in the left, yields contributions from the line integrals around the central singularity ($S_3 = -1$), and at $\rho\to\infty$ ($S_3 = +1$). On the Poincaré sphere, these integrals correspond to winding twice backward around the South and North pole, respectively, so Equation (7) evaluates to $n = \frac{1}{2}((-1)\cdot(-2) - 1\cdot(-2)) = 2$. Alternatively, we may choose $\mathbf{S}_R = (S_2, S_3, S_1)$ as illustrated in Figure 1c. This results in four singularities: two horizontally and two vertically polarized. The corresponding path on the Poincaré sphere is traversed twice, alternatingly winding around $S_1 = 1$ (β_1 and β_3) and $S_1 = -1$ (β_2 and β_4), with positive and negative winding numbers respectively, and no contribution from the periphery, again resulting in the correct $n = 2$. As anticipated, n counts how many times the polarization wraps around the Poincaré sphere, taking into account the sense of the winding direction. Unlike Equation (1) our topological expression requires neither derivatives nor integration but can be read directly from the polarization profile. We will demonstrate in the following by experiment and simulation that our definition can provide a significant increase in accuracy and precision.

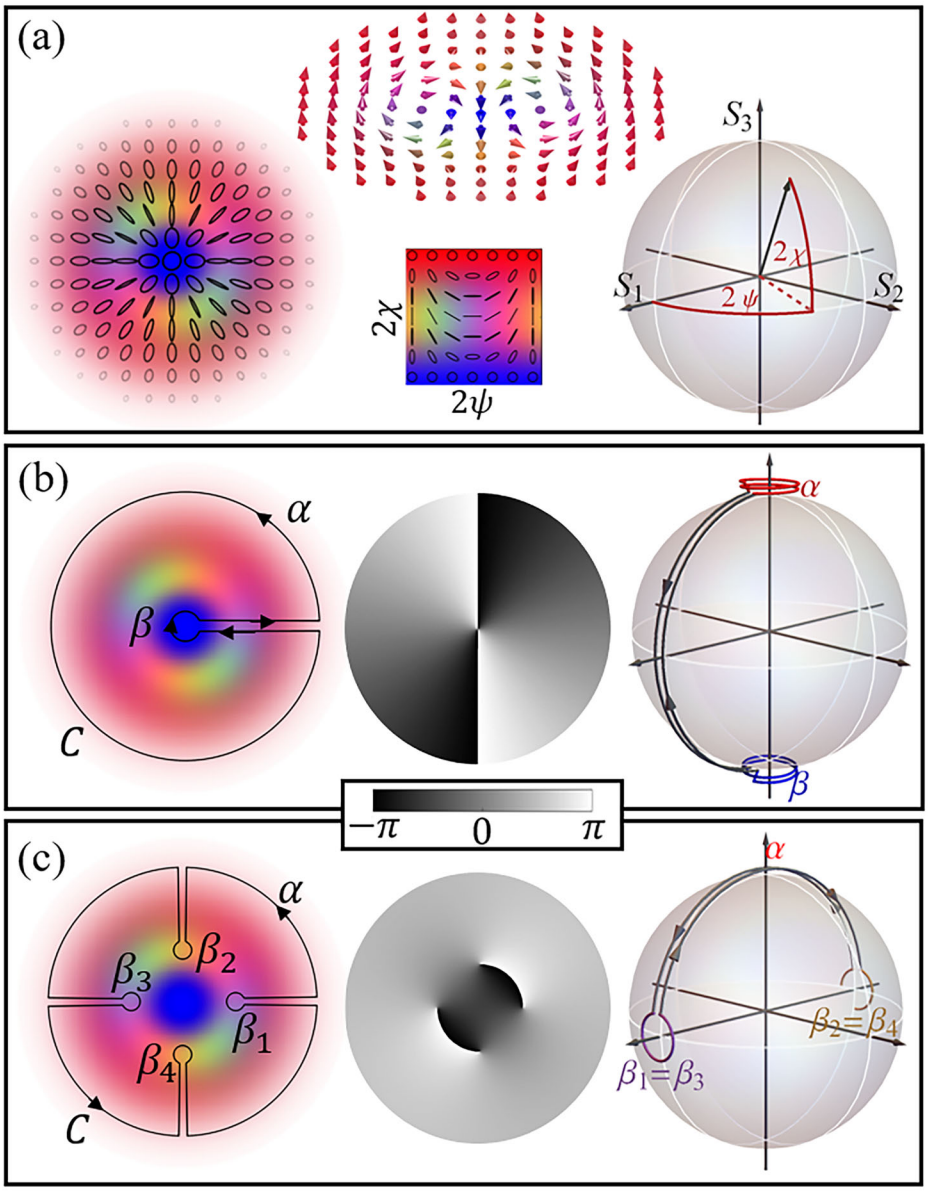

Figure 1. Topological measurement of the skyrmion number. a) Polarization profile, represented as a distribution of polarization ellipses and as a distribution of unitary Stokes vectors, of an $n = 2$ skyrmion. The associated Poincaré sphere is also shown, with ellipticity (χ) and orientation (ψ) angles indicated. The insert shows the polarization color scheme used, with intensity distribution represented as opacity. Path integrals (left), phase profiles Φ (center) and Poincaré spheres (right) evaluated for $S_z = S_3$ in (b) and $S_z = S_1$ in (c).

2.2. Experimental and Numerical Evaluation

When evaluating experimental data, the selection of the path is guided by fundamental as well as practical criteria: to obey Stokes's theorem, the enclosed area should contain as much as possible of the beam profile. For practical reasons, we want to choose a path that avoids areas of low intensity as well as the immediate neighborhood of the singularities, where measurements of the skyrmion field are dominated by noise.

In the following we will compare measurement methods Equation (1) and Equation (7) for skyrmions and bimerons[30] with various skyrmion numbers, as well as for multi-skyrmions.

A skyrmion with number n is conveniently generated as a superposition of orthogonally polarized Laguerre-Gaussian (LG) modes LG_p^{ℓ} (full expression given in Section SB, Supporting Information):[12]

$$|\Psi_n\rangle = \frac{1}{\sqrt{2}}\left(\mathrm{LG}_0^0|0\rangle + \mathrm{LG}_0^n|1\rangle\right) \tag{8}$$

Here p and ℓ denote the radial and azimuthal mode order respectively, and $|i\rangle$ with $i \in \{0, 1\}$ are any two orthogonal polarization states (i.e., a Schmidt basis). Choosing circular (linear) polarization basis states results in Néel-type skyrmions (bimerons).

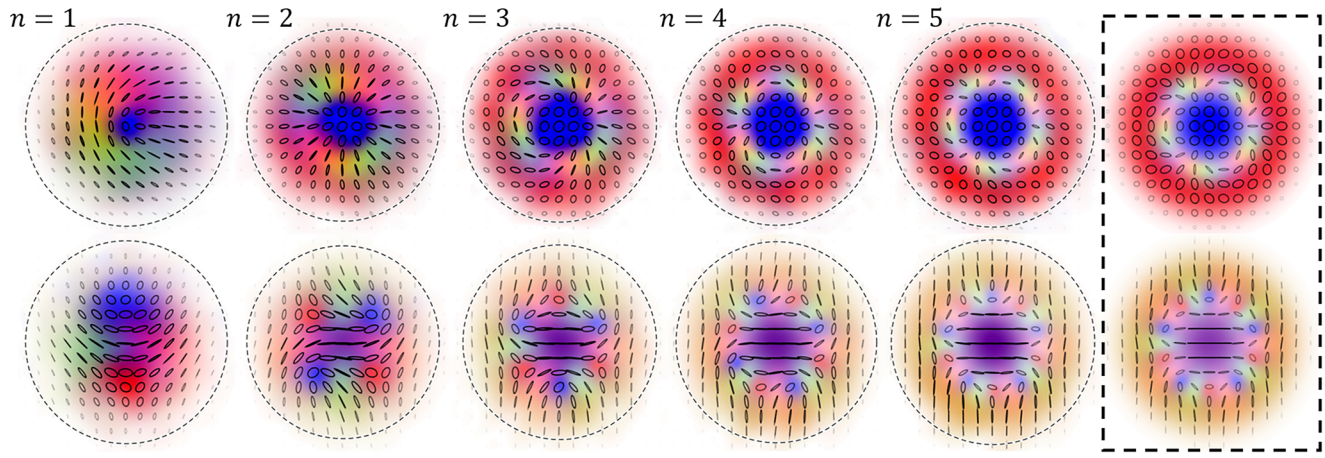

Figure 2. Experimentally measured polarization textures for beams with skyrmion numbers $n = 1$ to 5. The top row shows Néel-type skyrmions defined in the circular basis ($|0\rangle = |l\rangle$, $|1\rangle = |r\rangle$), and the bottom row Néel-type bimerons in the linear basis ($|0\rangle = |h\rangle$ and $|1\rangle = |v\rangle$). The inset at the right shows the theoretical polarization textures of the corresponding target skyrmions for $n = 5$.

Table 1. Comparison of experimentally measured skyrmion numbers for Figure 2 evaluated using Equation (1) and Equation (7), respectively.

type	method	$n = 1$	$n = 2$	$n = 3$	$n = 4$	$n = 5$
skyrmion	Equation (1)	0.918	1.921	2.994	4.007	4.924
	Equation (7) ($S_z = S_3$)	0.913	1.910	2.925	3.891	4.884
	Equation (7) ($S_z = S_1$)	1.000	1.998	2.994	3.989	4.976
bimeron	Equation (1)	0.927	1.941	2.971	3.999	4.991
	Equation (7) ($S_z = S_1$)	0.915	1.931	2.970	3.966	4.972
	Equation (7) ($S_z = S_3$)	1.000	1.998	2.992	3.989	4.993

We generate vector beams of the form Equation (8) by encoding the LG modes as multiplexed holograms on a digital micromirror device (DMD), following the procedure outlined in[31,32] and detailed in Supporting Information B. To characterize our vector beam, we take spatially resolved Stokes measurements, which can be processed to obtain spatially resolved polarization profiles, as illustrated in **Figure 2** for skyrmions and bimerons with $1 \leq n \leq 5$. These profiles show good qualitative agreement with the corresponding theoretical polarization profiles, as the reader can confirm by comparing the measured to the simulated $n = 5$ target skyrmions shown as inset in Figure 2.

The spatially resolved Stokes measurements $\mathbf{S}(x, y)$ also form the basis of a quantitative analysis of n according to the surface integral method Equation (1) and our topological method Equation (7), summarised in **Table 1**. To ensure a fair comparison between the methods, the experimentally measured Stokes images were cropped to a disk across which the intensity is $\leq 5\%$ of the peak intensity, as indicated by the dashed circles in Figure 2. Diffraction artefacts and noise were reduced by low-pass Fourier filtering the camera images.

Equation (1) evaluates the skyrmion number directly from the measured Stokes vectors $\mathbf{S}(x, y)$ and their numerical gradients. The surface integral was performed over the entire grid space.

Our topological method, Equation (7), requires us to identify $\bar{S}_z^{(\infty)}$ (here taken as the edge of the disk), $S_z^{(j)}$ and the corresponding winding numbers. In Table 1, we present the experimental results for $S_z = S_3$ and $S_z = S_1$, corresponding to the illustrations in Figure 1b,c, respectively.

With both methods we obtain a skyrmion number that closely matches the target value for each of the beams. We achieve the highest accuracy when evaluating Equation (7) in a mutually unbiased basis to the Schmidt basis that defines the skyrmion in Equation (8), i.e. using $S_z = S_1$ for Néel type skyrmions and $S_z = S_3$ for bimerons. This choice of generalized Stokes vectors shifts the relevant path integrals away from low intensity regions, where noise would compromise the evaluation of the Stokes parameters.

As the skyrmion number is a global beam property, defined either by integration over an infinite transverse plane, or from evaluating the Stokes parameter at an infinite radius, any measurement is necessarily an approximation. [Strictly speaking this applies only to skrymions constructed from spatial modes that are defined over an infinite plane as e.g. the LG modes used here or also Bessel modes]. Differences from the target skyrmion number arise from inaccuracies in the experimental generation process as well as the numerical evaluation. An artefact of our particular skyrmion 'recipe' as defined in Equation (7) is that, especially for Equation (1), accuracy improves for higher skyrmion numbers, as the intensity profile of the two constituting spatial modes LG_0^n and LG_0^0 overlaps less, so that $S_z^{(\infty)}$ is better defined.

Finally, we note that the obtained skyrmion number is influenced by the extent to which filtering is performed. Additional detail on the experimental generation and analysis methods are presented in Section SC (Supporting Information).

In our experiment, we have generated skyrmion beams with high fidelity, however in many situations, one may not have this luxury, e.g., when working at extremely low light levels, or when investigating light after propagation through noisy environments. It is perhaps no surprise that a topological identification of n proves more effective to tackle noise, whereas noise amplification is an inherent property for the differentiation required in Equation (1).

We have confirmed this by applying artificial background noise to simulated data, adding random noise levels ranging from 0 to

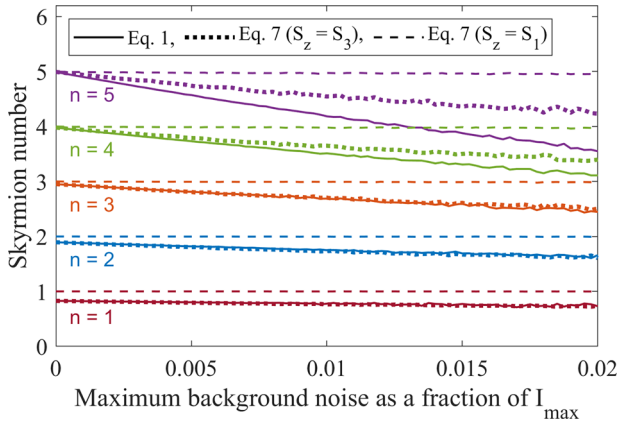

Figure 3. Comparison of skyrmion measurement methods for increasing noise levels. Background noise is applied to simulated Néel-type skyrmion beams with $n = 1$ to 5, and evaluation is performed over the disk where intensity exceeds 5% of the peak intensity. Solid lines indicate values calculated using Equation (1). Dotted lines are using Equation (7) in the Schmidt basis of the beam ($S_z = S_3$) and dashed lines show values when evaluating in an orthogonal polarization basis ($S_z = S_1$).

2% of the peak intensity I_{max} independently to each raw input image corresponding to the Stokes measurements. The resulting calculated Néel-type skyrmion numbers for beams with $n = 1$ to 5 (corresponding to the upper row of Figure 2) are shown in **Figure 3**. We find that noise leads to an underestimation of n for the integral method Equation (1) and less so for the topological method when evaluated in the Schmidt basis. Our simulations indicate that we can obtain an almost noise-free skyrmion number (shown by dashed lines in Figure 3) when choosing to evaluate Equation (7) using the mutually unbiased polarization basis. In addition, our simulations indicate an offset for low valued n numbers, which again disappears for topological evaluation in the orthogonal polarization basis.

2.3. Characterization of Multi-Skyrmions

In the remainder of this research article we will highlight the geometric interpretation of Equation (7) by discussing its application to multi-skyrmions.

We have seen that for individual skyrmions, a rotation of the Poincaré sphere leads to a different interpretation of the spin texture and its polarization singularities. For multi-skyrmions, it may also result in a different attribution of sub-skyrmion structures. We illustrate this with a multi-skyrmion ring,

$$|\Psi_{\text{ring}}\rangle = \frac{1}{\sqrt{2}}(\text{LG}_0^2\,|h\rangle - \text{LG}_0^5\,|v\rangle) \tag{9}$$

While such a ring of multi-skyrmions will be unfeasible in magnetic spin structures, optically we can generate more exotic skyrmion textures. The measured polarization texture of this multi-skyrmion structure is shown in the left of **Figure 4**. Based on the integral method (Equation (1)) we obtain an experimental skyrmion number of 2.918, close to the overall target value of $n = 3$. The topological method yields even more accurate skyrmion numbers of $n = 2.958$, $n = 2.996$, and $n = 2.998$ for $S_z = S_1$, S_2, and S_3, respectively. The associated phase profiles and integration paths are provided in Figure 4a–c.

For Figure 4a, $S_z = S_1$ coincides with the Schmidt basis of the multi-skyrmion as defined in Equation (9) and the only singularity appears at the centre of the beam profile. Figure 4b,c interprets the beam in terms of winding numbers around diagonal/antidiagonal and circular polarization singularities. The six singularities in the Stokes phase Φ, where $S_z \to \pm 1$ each represent a meron which contributes a skyrmion number of 1/2, with no contribution from the beam edge. The experimentally obtained skyrmion values obtained with $S_z = S_2$ and S_3 deviate from the ideal value of three only by about one°, an error reduced by an order of magnitude from that in the linear polarization basis. This arises from the higher accuracy in determining S_z at singularities positioned in beam areas of higher intensity, which could be confirmed by applying artificial noise to a simulated multi-skyrmion ring (details are provided in Section SD, Supporting Information), providing further evidence that a judicious choice of the generalised Stokes basis allows us to optimize measurement protocols. A detailed investigation over evaluation areas with varying radii reported in Section SE (Supporting Information) shows that the topological method, if applied in an orthogonal basis, yields the correct n as soon as all singularities are included within the evaluation area.

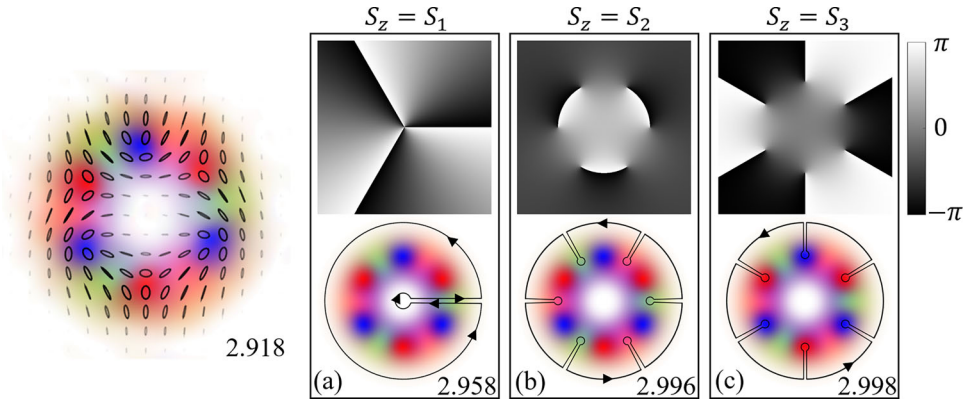

Figure 4. Interpretation of a multi-skyrmion in terms of different polarization bases. Left: experimentally measured polarization texture of the multi-skyrmion Equation (9), displaying n based on the integral method. Right: Phase Φ (top row) and integration path for a-c) $S_z = S_1,\ S_2,\ S_3$, respectively, displaying the corresponding experimentally obtained skyrmion number evaluated by the topological method.

3. Conclusion

In this research article, we have introduced a novel method for calculating the skyrmion number of paraxial optical skyrmion fields that captures the topological texture by line integration. While our method is expressed in terms of optical skyrmions, the principles apply to any 2D skyrmions, including e.g., magnetic skyrmions in thin films. We demonstrate excellent agreement between measured and theoretical skyrmion numbers for various examples of experimental skyrmion and bimeron beams constructed from superpositions of orthogonally polarized Laguerre-Gaussian modes. We demonstrate that our topological method, when evaluated for a suitably chosen basis, allows us to identify the correct skyrmion number at noise levels where the integral method would fail. Our method also facilitates the exploration of novel topological structures beyond individual skyrmions, as illustrated by the example of a multi-skyrmion. Research on optical skyrmions is still in its infancy. We anticipate that our new method to identify and assess the quality of experimental skyrmion fields directly benefits the growth of the discipline.

Supporting Information

Supporting Information is available from the Wiley Online Library or from the author.

Acknowledgements

The authors thank Sijia Gao for early discussions on the nature and properties of optical skyrmions. A.M. acknowledges financial support from the UK Research and Innovation Council via grant EPSRC/DTP 2020/21/EP/T517896/1. C.M.C., S.M.B., and S.F.-A. acknowledge financial support from the Royal Society through a Newton International fellowship NIF/R1/192384 and a Research Professorship RP150122. J.B.G acknowledges financial support from the EPSRC via grant EP/V048449/1 and the Leverhulme Trust.

Conflict of Interest

The authors declare no conflict of interest.

Data Availability Statement

The data that support the findings of this study are openly available in Enlighten at https://doi.org/10.5525/gla.researchdata.1400, reference number 1400.

Keywords

optical skyrmions, orbital angular momentum, skyrmions, topology, vector beams

Received: February 17, 2023
Revised: June 23, 2023
Published online: July 30, 2023

[1] T. H. R. Skyrme, B. F. J. Schonland, *Proc. R. Soc. A: Math. Phys. Eng. Sci.* **1961**, *260*, 127.
[2] P. Sutcliffe, *J. High Energy Phys.* **2010**, *2010*, 8.
[3] U. Al Khawaja, H. Stoof, *Nature* **2001**, *411*, 918.
[4] C. D. Parmee, M. R. Dennis, J. Ruostekoski, *Commun. Phys.* **2022**, *5*, 1.
[5] M. Rho, I. Zahed, *The Multifaceted Skyrmion*, 2nd ed., **2016**.
[6] A. N. Bogdanov, C. Panagopoulos, *Nat. Rev. Phys.* **2020**, *2*, 492.
[7] Y. Tokura, N. Kanazawa, *Chem. Rev.* **2021**, *5*, 2857.
[8] C. Back, V. Cros, H. Ebert, K. Everschor-Sitte, A. Fert, M. Garst, T. Ma, S. Mankovsky, T. L. Monchesky, M. Mostovoy, N. Nagaosa, S. S. P. Parkin, C. Pfleiderer, N. Reyren, A. Rosch, Y. Taguchi, Y. Tokura, K. von Bergmann, J. Zang, *J. Phys. D: Appl. Phys.* **2020**, *53*, 363001.
[9] S. Donati, L. Dominici, G. Dagvadorj, D. Ballarini, M. D. Giorgi, A. Bramati, G. Gigli, Y. G. Rubo, M. H. Szymańska, D. Sanvitto, *Proc. Natl. Acad. Sci. USA* **2016**, *113*, 14926.
[10] S. Tsesses, E. Ostrovsky, K. Cohen, B. Gjonaj, N. H. Lindner, G. Bartal, *Science* **2018**, *361*, 993.
[11] L. Du, A. Yang, A. Zayats, X. Yuan, *Nat. Phys.* **2019**, *15*, 650.
[12] S. Gao, F. C. Speirits, F. Castellucci, S. Franke-Arnold, S. M. Barnett, J. B. Götte, *Phys. Rev. A* **2020**, *102*, 053513.
[13] S. Gao, F. C. Speirits, F. Castellucci, S. Franke-Arnold, S. M. Barnett, J. B. Götte, *Phys. Rev. A* **2021**, *104*, 049901.
[14] D. Sugic, R. Droop, E. Otte, D. Ehrmanntraut, F. Nori, J. Ruostekoski, C. Denz, M. R. Dennis, *Nat. Commun.* **2021**, *12*, 1.
[15] Y. Shen, E. C. Martínez, C. Rosales-Guzmán, *ACS Photonics* **2022**, *9*, 269.
[16] J. Zhu, S. Liu, Y.-S. Zhang, arXiv:2103.11293v2 [quant-ph], **2021**.
[17] X. Lei, A. Yang, P. Shi, Z. Xie, L. Du, A. V. Zayats, X. Yuan, *Phys. Rev. Lett.* **2021**, *127*, 23.
[18] X. Pang, H. Zhang, M. Hu, X. Zhao, *IEEE Photonics J.* **2022**, *14*, 1.
[19] Y. Shen, B. Yu, H. Wu, C. Li, Z. Zhu, A. V. Zayats, *Adv. Photonics* **2023**, *5*, 01.
[20] C. Cisowski, C. Ross, S. Franke-Arnold, *Adv. Photonics Res.* **2023**, *4*, 2370007.
[21] N. Rivera, I. Kaminer, *Nat. Rev. Phys.* **2020**, *2*, 538.
[22] A. Bogdanov, A. Hubert, *J. Magn. Magn. Mater.* **1994**, *138*, 255.
[23] R. Gutiérrez-Cuevas, E. Pisanty, *J. Opt.* **2021**, *23*, 024004.
[24] Y. Shen, Q. Zhang, P. Shi, L. Du, A. V. Zayats, X. Yuan, arXiv:2205.10329v1 [physics.optics], **2022**, 1.
[25] N. Nagaosa, Y. Tokura, *Nature Nanotech.* **2013**, *8*, 899.
[26] D. Foster, C. Kind, P. J. Ackerman, J.-S. B. Tai, M. R. Dennis, I. I. Smalyukh, *Nat. Phys.* **2019**, *15*, 655.
[27] N. D. Mermin, T.-L. Ho, *Phys. Rev. Lett.* **1976**, *36*, 594.
[28] R. D. Kamien, *Rev. Mod. Phys.* **2002**, *74*, 953.
[29] M. R. Dennis, K. O'Holleran, M. J. Padgett, *Chapter 5 Singular Optics: Optical Vortices and Polarization Singularities*, vol. *53*, Elsevier, Amsterdam **2009**.
[30] Y. Shen, *Opt. Lett.* **2021**, *46*, 3737.
[31] A. Selyem, C. Rosales-Guzmán, S. Croke, A. Forbes, S. Franke-Arnold, *Phys. Rev. A* **2019**, *100*, 063842.
[32] C. Rosales-Guzmán, X. B. Hu, A. Selyem, P. Moreno-Acosta, S. Franke-Arnold, R. Ramos-Garcia, A. Forbes, *Sci. Rep.* **2020**, *10*, 1.